geosciences

MDPI

Article

Deep Structural Characteristics and Favorable Hydrocarbon Zone Prediction in the Southwestern Tarim Basin

Lei Wen [1,2], Depeng Zhu [1,2], Yingjie Liu [1,2], Weize Ma [1,2,*], Yunlu Xin [1,2,*] and Youxing Yang [1,2]

[1] Oil & Gas Survey, China Geological Survey, Beijing 100083, China
[2] State Key Laboratory of Continental Shale Oil, Beijing 100083, China
* Correspondence: maweize@mail.cgs.gov.cn (W.M.); xinyunlu@mail.cgs.gov.cn (Y.X.)

Abstract

The deep structural characteristics and distribution of favorable hydrocarbon zones in the Southwestern (SW) Tarim Depression, a first-order tectonic unit of the Tarim Basin, remain unclear, restricting oil and gas exploration progress. To reveal the deep geological structure and predict favorable hydrocarbon zones, this paper systematically analyzes the resistivity and polarizability characteristics of the depression using a ~236 km composite Time-Frequency Electromagnetic (TFEM) profile formed from 60.6 km newly acquired and 175.4 km reprocessed legacy data. The resistivity inversion profile clearly delineates a north–south "three-zone" structural pattern of the Lower Paleozoic in the study area: the southern West Kunlun thrust belt exhibits imbricate thrust nappe structures; the central Yecheng sag is a deeply buried depression thickening southward; and the northern Maigaiti slope is a broad gentle slope rising northward. Furthermore, the TFEM profile clearly depicts NE-trending Precambrian aulacogens controlled by normal faults, filled with Nanhua–Sinian strata locally exceeding 1500 m in thickness. Combined analysis of the 20 strong (Class I and II) polarizability anomalies identified along the profile and the resistivity structures indicates that favorable hydrocarbon zones are mainly distributed in the intra-sag uplift anticline belt within the Yecheng sag and the faulted anticline development belt in the middle section of the Maigaiti slope. The most favorable exploration layers are the Carboniferous and Permian, with the Silurian–Devonian as a potential replacement series. This study demonstrates that TFEM can effectively identify deep resistivity and polarizability anomalies, and the "structure-fluid" superposition relationship revealed provides a new exploration direction for the SW Tarim Depression.

Keywords: Southwestern Tarim Basin; Time–Frequency Electromagnetic Method; deep structure; Precambrian aulacogen; Hydrocarbon Favorable Zone Prediction

Check for updates

Academic Editor: Olivier Lacombe

Received: 10 October 2026
Revised: 20 November 2026
Accepted: 22 November 2026
Published: 24 November 2026

Copyright: © 2026 by the authors. Licensee MDPI, Basel, Switzerland. This article is an open access article distributed under the terms and conditions of the Creative Commons Attribution (CC BY) license.

1. Introduction

The Tarim Basin is a large superimposed composite petroliferous basin in western China. The Southwestern (SW) Tarim Depression, a first-order tectonic unit of the Tarim Basin, has a vast area and great hydrocarbon exploration potential, but the overall exploration degree is low. In particular, the unclear deep geological structure and distribution of favorable hydrocarbon zones have hindered exploration breakthroughs [1–3]. In recent years, wells Luotan 1 and Yetan 1 have successively achieved high-yield oil and gas flows, confirming that this area has good hydrocarbon resource potential. However, most existing discoveries are concentrated in the piedmont zone or high parts of the slope, whereas no major breakthrough has been made in the deeply buried core of the depression [4].

Therefore, it is urgent to carry out detailed characterization of deep structures and prediction of favorable zones.

Previous studies have carried out extensive work on the tectonic evolution [5–8], stratigraphic development [9,10], and source rock characteristics [11,12] of the SW Tarim Depression, laying a solid foundation for basic geological research. Yang Haijun et al. [4] systematically summarized the exploration progress of the Tarim Basin during the "14th Five-Year Plan" period, pointing out that near-source exploration is the main target. It is generally believed that this area has experienced multiple stages of complex tectonic superimposition and reworking and developed multiple sets of source rocks, including the Cambrian, Carboniferous, Permian, and Jurassic [3,11,13]. Nevertheless, three geological problems remain unresolved in this area: (1) the distribution, structural style, and sedimentary fill of the Precambrian rift system are poorly constrained owing to the limited quality of deep seismic data; (2) although the three major structural units are already well recognized, the deep three-dimensional geometry of the Lower Paleozoic—such as the burial depth of the sag and its thickening pattern—still lacks quantitative constraints; and (3) no direct geophysical evidence is available for identifying favorable deep hydrocarbon zones. The contribution of this study is therefore not to "discover" new structural units but to provide new quantitative electrical constraints on, and to refine, the previously established structural framework using TFEM data.

The Time–Frequency Electromagnetic Method (TFEM) integrates the advantages of time-domain and frequency-domain methods. It can obtain multi-parameter information, including resistivity and polarizability, in a single acquisition, showing good application prospects in oil and gas exploration [14–16]. Resistivity parameters can effectively reveal stratigraphic structure, tectonic morphology, and fault characteristics, while polarizability anomalies can serve as a potential indicator of hydrocarbon accumulation; however, this indication is subject to mineralogical and electrochemical ambiguity and therefore needs to be evaluated jointly with structural traps, with interference from electron-conductive minerals such as pyrite excluded [17].

To break through this bottleneck, this study relies on the TFEM exploration work deployed by the Oil & Gas Survey, China Geological Survey in the SW Tarim Depression, combined with regional gravity and magnetic data, aiming to (1) improve the characterization accuracy of deep structures and fault distribution within the previously established structural framework using high-precision resistivity inversion; (2) delineate hydrocarbon-related anomalies based on polarizability and other parameters, and propose preliminary targets of favorable exploration zones and series, providing a geophysical basis for further oil and gas survey and well deployment in this area.

The poor quality of deep seismic imaging in the SW Tarim Depression results from a combination of factors: the great thickness of Cenozoic and Mesozoic strata in the piedmont zone strongly attenuates seismic energy; complex thrust deformation distorts the wavefield and hampers migration imaging; and the weak impedance contrasts beneath the Cambrian, compounded by multiples, yield low signal-to-noise reflections from the Lower Paleozoic and Precambrian. Consequently, the structural characteristics, fault distribution, and sedimentary fill of these deep intervals remain poorly constrained [8,18], restricting the understanding of deep hydrocarbon accumulation conditions. Electromagnetic methods offer a complementary physical basis: they sense resistivity contrasts rather than acoustic impedance and are therefore insensitive to the seismic energy attenuation that degrades deep reflections. The study area exhibits favorable electrical contrasts—high-resistivity Cambrian–Ordovician carbonates against overlying low-resistivity clastics, and low-resistivity sedimentary fills within Precambrian aulacogens —making deep structures electrically distinguishable even where seismic imaging fails. In particular, the Time–

Frequency Electromagnetic Method (TFEM), with its high-power source and low-frequency content, achieves investigation depths exceeding 10 km, while joint time–frequency processing suppresses noise and reduces inversion non-uniqueness [14–17,19]. Although its lateral resolution is lower than that of seismic data at shallow depths, TFEM provides effective constraints on deep electrical structures where seismic data are of limited quality. To our knowledge, the composite TFEM profile formed in this study is the first TFEM profile of such length in the SW Tarim Depression that depicts the deep structural characteristics of the whole depression.

2. Geological Setting

The SW Tarim Depression is located on the southwestern margin of the Tarim Basin, bordering the Bachu Uplift to the north and the West Kunlun orogenic belt to the south (Figure 1). It is a superimposed depression controlled by multiple tectonic movements and can be divided from south to north into three second-order structural units: the West Kunlun thrust belt, the Yecheng sag, and the Maigaiti slope [5,7]. The Maigaiti slope is a long-lived south-dipping broad gentle slope with east–west segmentation in its tectonic evolution: the western part turned south-dipping after the Carboniferous, favoring long-term northward migration and accumulation of oil and gas, forming early oil reservoirs and late gas reservoirs; the eastern part only underwent tilt reversal in the Miocene, dominated by late-stage accumulation [20]. The piedmont of the Yecheng sag has undergone complex deformation, developing multiple en echelon short-axis anticline belts with deformation intensity decreasing from south to north [5]. The West Kunlun thrust belt is a strongly active thrust nappe system since the Cenozoic, with multi-phase and spatiotemporal differences in activity [21].

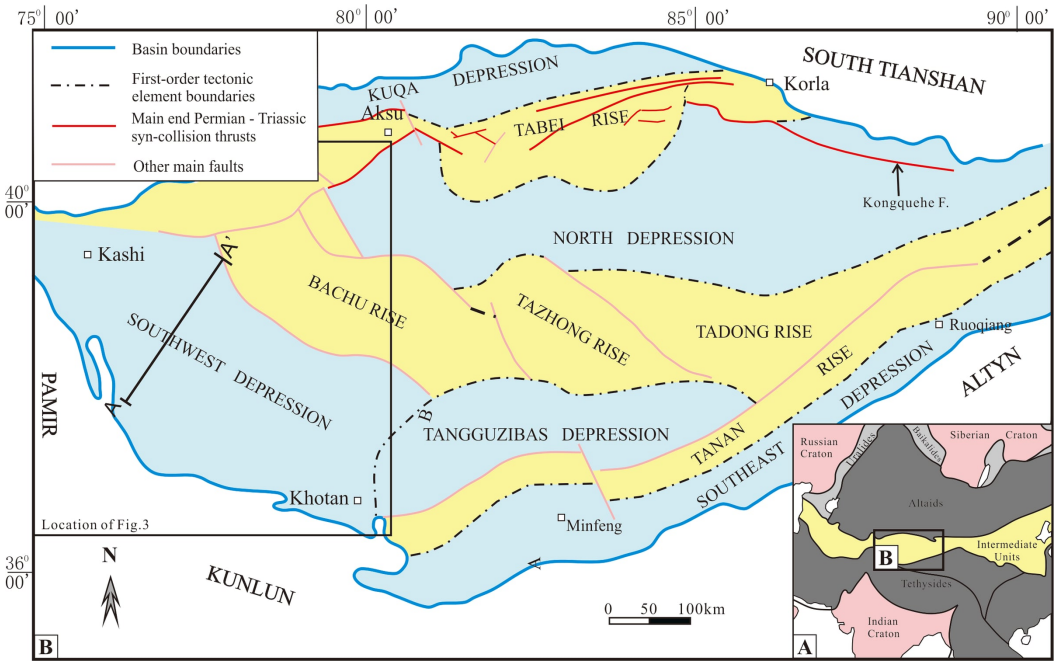

Figure 1. Tectonic unit division map of the Tarim Basin. (**A**) Geological Structure Map of Central Asia; (**B**) Map of Structural Units in the Tarim Basin.

The geological structure of the SW Tarim Depression is characterized by a complex superposition of Paleozoic cratonic and Meso-Cenozoic foreland sequences. The regional geological map (Figure 1B) shows that the depression is bounded by the West Kunlun fault to the south and the Bachu fault to the north, with several secondary faults developed

internally. The geological cross-section (Figure 2) illustrates the typical structural style: the southern part is dominated by basement-involved thrusts forming imbricate fans, the central part is a deep sag with relatively undeformed strata, and the northern part is a gently dipping slope with minor normal faults. This architecture strongly controls the distribution of source rocks, reservoirs, and cap rocks.

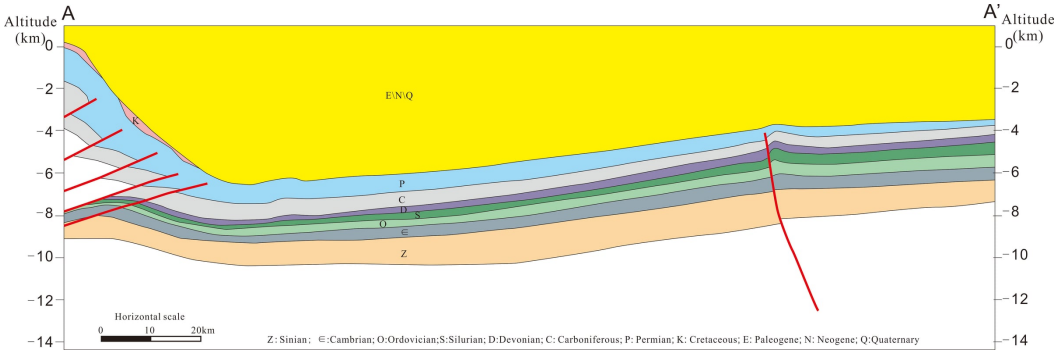

Figure 2. Geological cross-section (A–A′) across the SW Tarim Depression (according to [22]).

The SW Tarim Depression has deposited a huge thickness of strata from the Sinian to the Quaternary, generally showing a superimposed sedimentary feature of Paleozoic marine carbonate platforms and Meso-Cenozoic continental foreland basins. The Cambrian–Ordovician is dominated by platform facies carbonates with great thickness, serving as important reservoirs [9]; the Silurian–Devonian consists of littoral–neritic clastic rocks; the Carboniferous–Permian comprises marine and marine-terrigenous interbedded carbonates and clastic rocks, with the Carboniferous being a regionally developed important source rock [13]; the Mesozoic (Cretaceous) is mainly distributed in the piedmont zone [11]. Regional cap rocks include the Middle Cambrian gypsum-salt rock, Carboniferous mudstone, and Paleogene gypsum-mudstone, forming multiple excellent reservoir-cap assemblages with the underlying reservoirs [3].

However, the deep seismic data in the SW Tarim Depression are characterized by low resolution and poor imaging quality, particularly below the Cambrian, because seismic energy is strongly attenuated by the thick Cenozoic and Mesozoic strata and complex tectonic deformation. As a result, the Precambrian rift system remains poorly constrained, and its distribution, structural style, and sedimentary fill are still unclear [8,18]. This limitation has hindered the understanding of deep hydrocarbon accumulation conditions and the evaluation of Precambrian exploration potential, making it necessary to introduce electromagnetic methods with greater penetration depth and sensitivity to electrical contrasts.

3. Materials and Methods

3.1. Principle of TFEM

TFEM adopts an equatorial dipole device, transmitting a series of square wave currents into the subsurface through a high-power transmitter and receiving the electric field (E_x) and vertical magnetic field (dBz/dt) components at the surface [14,23]. Its core technical advantage lies in acquiring both time-domain (pure secondary field) and frequency-domain (total field) data in a single acquisition. The time-domain data are used for resistivity inversion to reveal subsurface electrical structures; the frequency-domain data are used to invert parameters such as polarizability (η) and time constant (τ) based on the Cole–Cole complex resistivity model [24]. These parameters are closely related to the fluid properties of reservoir pores; however, because induced-polarization and complex-resistivity responses can be affected by various electrochemical and mineralogical processes, high polarizability

anomalies should be regarded as a potential indicator of hydrocarbon accumulation rather than a direct diagnostic of oil and gas reservoirs [17].

The characteristics of hydrocarbon reservoirs in electrical exploration are manifested as elevated resistivity of the reservoir and high conductivity around the reservoir. In addition, calcification and secondary pyritization of the reservoir, as well as the electrical double layer at the oil-water interface in pore spaces, can generate strong induced polarization anomalies. The joint time–frequency dual-domain processing effectively suppresses non-uniqueness and improves the detection accuracy of deep targets [15,19]. It should be noted that such electrical and induced-polarization responses are not unique to hydrocarbon reservoirs: similar anomalies can also be produced by clay content, disseminated sulfide minerals, and near-surface interference, so they cannot be used alone as diagnostic characteristics of hydrocarbon reservoirs.

3.2. Data Acquisition and Processing

In this study, five new TFEM profiles were acquired, totaling 60.6 km with a station spacing of 200 m. Additionally, 175.4 km of legacy TFEM and magnetotelluric sounding data were reprocessed. Finally, a north–northeast-trending large grid profile (approximately 236 km long) was formed by splicing (Figure 3).

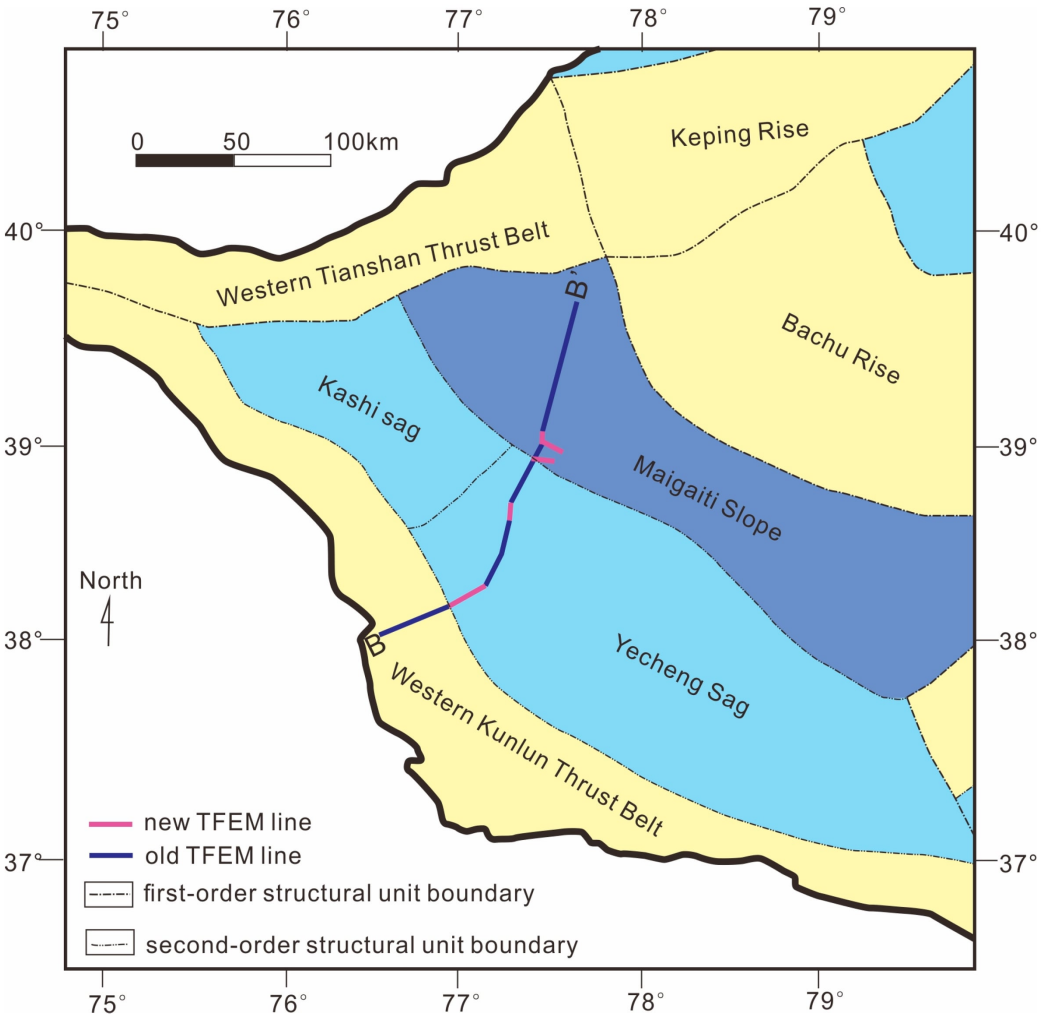

Figure 3. Tectonic unit division and TFEM line deployment map of the SW Tarim Depression.

The legacy data involved in this study were acquired in four campaigns with different instruments and acquisition parameters: the 2006 Maixi MT (controlled-source audio-

frequency) survey, the 2008 Shache–Pishan MT survey, the 2020 Qimeigan TFEM survey, and the 2023 Maigaiti–Shache TFEM survey. Because the data span a long period of time, they differ considerably from batch to batch: the MT data were acquired mainly with AGE-xxl electromagnetic instruments, whereas the TFEM data were acquired with the TFEM-3 transmitter and Hawk receivers, and the excitation parameters vary greatly among batches, making data splicing difficult. The newly acquired lines connect with the legacy lines at their ends, which provides overlapping segments for consistency checks between the multi-batch datasets. A total of 274.2 km of legacy data were recompiled and reprocessed in this project. Limited by the acquisition accuracy and parameters of the instruments at that time, the reprocessed legacy data have relatively low resolution and reliability for deep information; the north–south-trending line segments were therefore spliced with smoothing applied at the joints to eliminate systematic offsets between batches, forming a 236 km composite profile consisting of 60.6 km of newly acquired TFEM data and 175.4 km of selected reprocessed legacy data.

The reprocessing of the legacy data employed the following key techniques:

(1) High-fidelity preprocessing: Multi-cycle stacking noise suppression, background noise elimination, and fixed-period interference notch filtering were applied to the acquired data to preserve more weak signals.
(2) Harmonic extraction: Harmonics were extracted from the original frequency-domain data during reprocessing, which increased the data volume in the frequency domain and enhanced the vertical resolution of the profiles.
(3) Full-frequency processing: The reprocessing adopted a frequency-domain approach using the GeoGME software, in which all acquired data were involved in the computation, thereby improving the resolution of the data. GeoGME is a gravity–magnetic–electrical processing system developed by BGP Inc. on the GeoEast platform, providing multiple inversion methods (e.g., OCCAM and simulated annealing) and widely used in non-seismic exploration.
(4) Integration with well data: The reprocessed profiles were inverted from an elevation of −9 km down to −12 km, and the calibrated horizons are more consistent with the new geological understanding. The inversion interval from an elevation of −9 km down to −12 km was selected because it covers the deeply buried Lower Paleozoic–Precambrian target section of the study area.
(5) Inversion: Resistivity and polarizability inversion was performed with the GeoGME software on the GeoEast platform. For the resistivity inversion, an OCCAM regularized inversion based on direct field values was adopted: the objective function combines the data misfit with a model-roughness (smoothness) penalty, the two terms being balanced by a Lagrange multiplier (regularization factor). The initial model was a layered geoelectric model constructed from the apparent resistivity curves together with the regional resistivity statistics of well logs, so that the inversion is relatively insensitive to the starting model. In each iteration the Lagrange multiplier was adjusted so that the normalized misfit (χ^2) approached the target value, and the inversion was judged to have converged when the misfit reached the predefined threshold and the model change between successive iterations became negligible. To verify the stability of the results, inversions with different initial models and regularization factors were compared, and the main structural features were consistently recovered. For the polarizability inversion, the geometric resistivity model obtained above was fixed, and the polarizability parameters were inverted under the Cole–Cole model; given the limited stability of the time constant and frequency exponent in this dataset, only the polarizability (η) is used in the subsequent analysis.

4. Results

4.1. Resistivity Profile Structure and Geological Interpretation

Based on the deep lateral resistivity logging curves of wells in and around the area (Figure 4), the correlation between resistivity and geological horizons was established. The well-tie profile clearly shows (1) a high-resistivity layer at the bottom of the Paleogene (E), significantly higher than the underlying strata (Mesozoic (Mz) or Permian (P)); (2) the Mesozoic (Mz) is developed in the West Kunlun thrust belt, with relatively low resistivity compared to the overlying and underlying strata; (3) the Permian (P) exhibits low resistivity compared to the underlying Carboniferous (C); (4) the Carboniferous (C) shows relatively high resistivity; (5) the Silurian–Devonian (S-D) shows relatively low resistivity; (6) the Cambrian–Ordovician (Є-O) shows distinctly high resistivity; (7) the Precambrian shows relatively low resistivity. Using this calibration result, detailed geological interpretation was carried out on the spliced north–northeast-trending large grid profile (Figure 5). Specifically, the correlation was established as follows: deep lateral resistivity logging curves of 40 wells that penetrated the Cambrian in the Tarim platform-basin area were compiled to obtain the resistivity statistics of each stratigraphic interval, and these statistics show that the resistivity of each layer is laterally consistent, varying only slightly across the basin; together with physical-property measurements (density and magnetic susceptibility) of core samples from 147 wells, they were cross-validated against regional geology and seismic horizons to establish the "electrical layer–geological layer" correspondence, by which nine electrical layers were identified in the study area. Ten wells along and around the survey lines (Kuntan 1, Jia 2, Qu 3, Qun 4, Qun 5, Qun 6, Qun 601, Qiong 001a, Qiong 002, and Qiong 003) were used for horizon calibration of each line; in segments without well control, the electrical marker layers were traced along the whole profile on the basis of the optimized electrical layering results combined with seismic data.

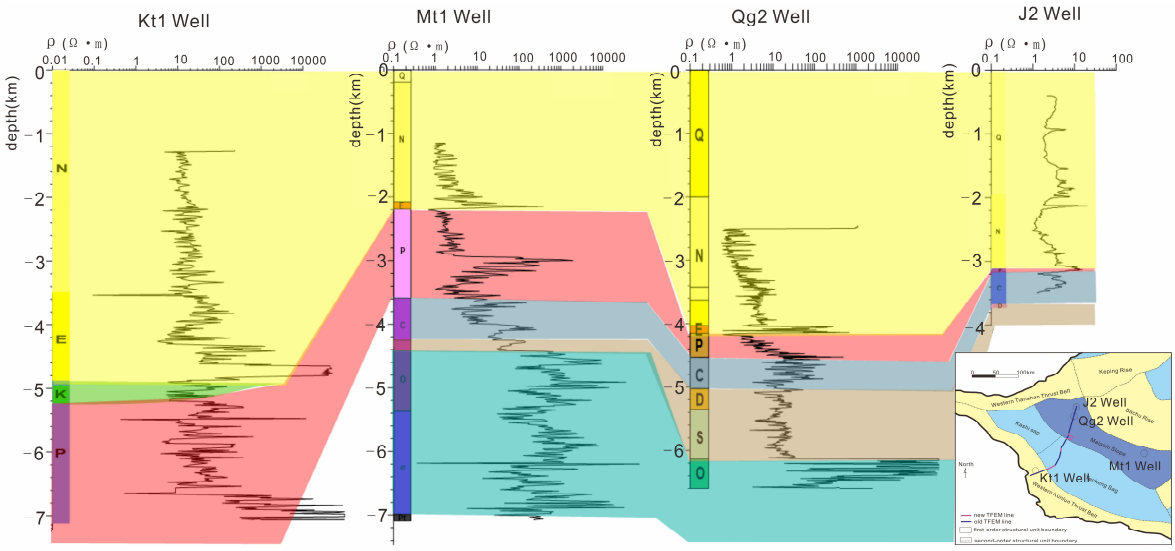

Figure 4. Key well electrical calibration profile in the SW Tarim Depression.

It should be emphasized that well-log measurements (centimeter- to meter-scale resolution, investigating a limited volume around the borehole) and TFEM-derived resistivity (tens- to hundreds-of-meters resolution, investigating a much larger volume) are not directly comparable point by point; the calibration adopted here is therefore a statistical correspondence at the level of electrical intervals rather than a point-by-point numerical comparison. Accordingly, integrated reservoir characterization studies are cited in this paper only as methodological and geological analogies, not as direct evidence for the electrical properties

of the Tarim formations. It should also be noted that different lithologies may exhibit similar resistivity (electrical equivalence), and the smoothness constraint of the inversion blurs boundary positions; therefore, in segments without well or seismic control, the resistivity boundaries are regarded as geological interpretations rather than determinations, with an associated depth uncertainty.

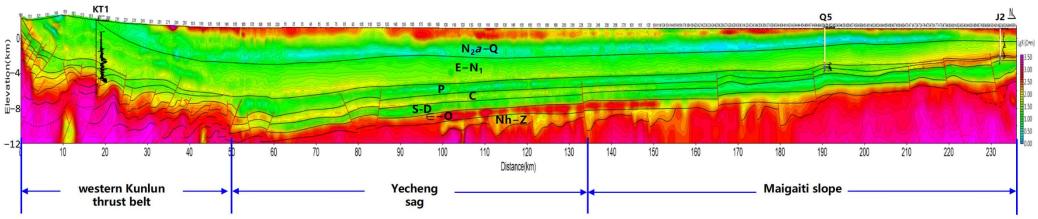

Figure 5. Resistivity inversion and comprehensive geological interpretation of the north–northeast-trending large grid profile in the SW Tarim Depression.

The resistivity profile clearly reveals a north–south "three-zone" structure of the Lower Paleozoic in the SW Tarim Depression (Figure 5).

Southern West Kunlun thrust belt: This zone is characterized by a series of north-dipping imbricate thrust faults with repeated strata. Paleozoic and Mesozoic strata are developed but strongly reworked by faults. The high-resistivity Cambrian–Ordovician bodies are cut into multiple fault blocks.

Central Yecheng sag: A half-graben-like depression that is deep in the south and shallow in the north. Faults are not developed inside the sag, and the structure is relatively stable. The Precambrian (Nh-Z) exhibits relatively low resistivity and contains internally wedge-shaped bodies bounded by normal faults, with a thickness of over 1500 m, interpreted as Nanhua–Sinian aulacogen deposits (Figure 5). This feature is consistent with the Nanhuaian rift system identified by Li Yong et al. [18] and Tian Lei et al. [8] based on seismic data, and the TFEM profile further finely characterizes the electrical structure of the aulacogen.

It should be noted that a wedge-shaped conductive body bounded by apparent structural discontinuities is not by itself sufficient evidence for an aulacogen: similar electrical configurations could also arise from lithological heterogeneity of the basement, deep weathering or alteration of the basement, conductive sedimentary successions of various ages, basement shear zones, or fluid alteration along fault zones. The direct geophysical observations here are the wedge-shaped geometry of the deep low-resistivity bodies, the resistivity contrasts across their bounding faults, and their depth and thickness. The geological inference that these wedge-shaped low-resistivity bodies represent Nanhua–Sinian aulacogen (rift trough) deposits is based mainly on two lines of geological evidence: (1) the deep wedge-shaped low-resistivity bodies, bounded by a series of normal faults, are morphologically similar to the rift system interpreted from seismic data in this region [18]; and (2) regional tectonic background analysis indicates that such wedge-shaped sedimentary bodies, composed of a series of normal-fault-bounded depocenters, should have formed under a regional extensional tectonic setting, which is consistent with the Nanhua–Sinian rifting event recorded around the Tarim Basin [8,18,25]. The thickness estimate (locally exceeding 1500 m) is derived from the inverted depths of the resistivity interfaces combined with regional depth-conversion assumptions, with an uncertainty on the order of several hundred meters. Furthermore, because a single 2-D resistivity section cannot determine the regional strike, lateral continuity, or plan-view orientation of a fault-bounded basin, the NE strike of the interpreted aulacogens is not inferred from the apparent geometry of the TFEM section; it is constrained by regional structural analysis, including residual gravity

and aeromagnetic anomaly trends, previous seismic interpretations (e.g., the TXN-GJX07 regional seismic profile), and the regional fault system [6,8,18,25]. The TFEM profile was deployed approximately perpendicular to the inferred strike, so that fault-bounded wedge geometries are expected to appear on the section.

Northern Maigaiti slope: Strata gradually rise and thin northward, forming a broad, gentle monoclinal form. Multiple northward-thrusting faults are developed, forming fault terraces. The Precambrian also shows aulacogen features, but with thinner thickness than in the Yecheng sag, and local upward piercing of high-resistivity basement is observed. This high-resistivity body could be interpreted as a mafic igneous intrusion; however, alternative explanations—such as an uplifted block of old crystalline basement or a dense carbonate block—cannot be excluded with the present data.

Multiple Precambrian aulacogens are developed in the SW Tarim Depression, among which the aulacogen in the central Maigaiti slope is the most reliable, clearly displayed on the resistivity profile. These aulacogens have a large residual thickness of Nanhua–Sinian strata and represent new deep exploration targets worthy of attention [8,18]. He Bizhu et al. [25] suggested that these aulacogens are extensional structures formed within the Tarim Craton during the breakup of the Rodinia supercontinent, genetically related to the regional "triple rift" system. Integrated analysis of residual gravity anomalies and the resistivity inversion profiles indicates that the aulacogens in the central part of the study area are the most reliable, being visible in both datasets, whereas the aulacogens interpreted in the northern and southern parts are supported mainly by gravity anomalies and remain less certain.

4.2. Polarizability Anomaly Characteristics and Hydrocarbon Favorable Zone Prediction

Polarizability (η, dimensionless) anomalies are regarded in this study as a potential indicator of hydrocarbon accumulation, subject to mineralogical and electrochemical ambiguity, rather than a direct indicator of oil and gas reservoirs [17]. The grading standard for polarizability anomalies adopted in this study is as follows: Class I anomaly ($\eta > 0.235$) represents high hydrocarbon potential, and Class II anomaly ($0.214 < \eta < 0.235$) represents good hydrocarbon potential. These thresholds were calibrated by BGP Inc., CNPC based on the TFEM polarizability statistics of dozens of wells in the Tarim Basin [26]; they are regional empirical thresholds and are cited in this study. If applied to other areas or other datasets, these thresholds cannot be used directly and must be recalibrated with local well data.

The spliced polarizability inversion profile (Figure 6) shows a total of 20 strong polarizability anomalies (Class I and II) developed across the whole profile, distributed in multiple layers. The anomalies are mainly concentrated in two areas:

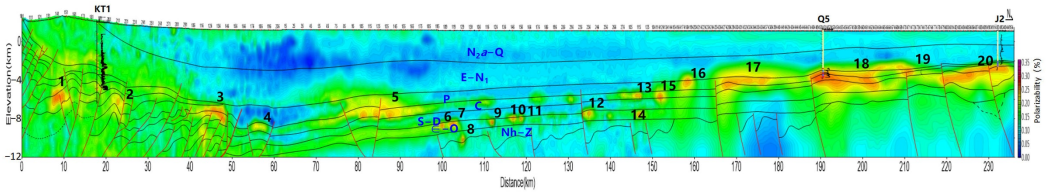

Figure 6. Polarizability (η) inversion and anomaly distribution of the north–northeast-trending large grid profile in the SW Tarim Depression (anomaly Nos. 1–20).

Yecheng sag: A Class I polarizability anomaly (No. 5) is developed at a local structural high (intra-sag uplift anticline) within the sag, located in the Carboniferous–Permian, well superimposed with the "intra-sag uplift" structure interpreted from the resistivity profile (Figure 6).

Maigaiti slope: Multiple strong polarizability anomalies (Nos. 17, 18, 19, 20, etc.) are developed, among which Nos. 17, 18, and 20 have high intensity and large extent, and are closely related to faults or local anticlinal structures. These anomalies are mostly located near structural hinge zones [13,20], indicating that stable areas during paleo-uplift migration are favorable for hydrocarbon enrichment.

Comprehensive evaluation suggests that the intra-sag uplift anticline in the Yecheng sag (anomaly No. 5) and the faulted anticline development belt in the middle section of the Maigaiti slope (anomaly Nos. 17, 18, 20) are the most favorable hydrocarbon exploration targets. Polarizability anomalies are most concentrated and strongest in the Carboniferous and Permian, indicating that these two series are the most realistic and favorable exploration layers at present. In addition, some intervals of the Silurian–Devonian also show Class II anomalies, serving as potential replacement series. The preference for the Carboniferous–Permian intervals is based on the observation that the polarizability anomaly values are highest and the anomaly zones are most numerous in these intervals. It should be emphasized that a comprehensive evaluation of favorable zones would require full consideration of source rock, reservoir, seal, trap, migration, and preservation conditions; this study, however, focuses on identifying the favorable zones indicated by TFEM data, and a full petroleum-system analysis is beyond its scope. In fact, numerous oil and gas fields have been discovered in the SW Tarim Depression, and recent drilling breakthroughs confirm that the basic petroleum geological conditions are present in this area.

5. Discussion

5.1. Data Reliability and Noise Suppression

To address the interference in this survey area, which is mainly concentrated in the high-frequency part (e.g., from high-voltage power lines), frequency-specific filtering was applied using GME-CS. The data quality was significantly improved after editing, as shown in Figure 7.

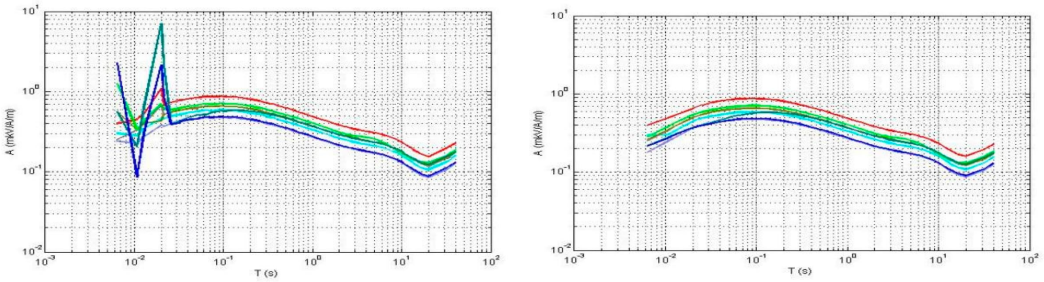

Figure 7. Comparison of original data amplitude curves before and after filtering (**left**: before filtering; **right**: after filtering). Different curves represent the signals from different receiving points.

5.2. Reliability and Multiplicity of Polarizability Anomalies

Polarizability anomalies are important bases for predicting hydrocarbon potential, but their multiplicity must be noted. Although the calibration using existing wells in the area has improved the reliability of anomaly interpretation, it may still be affected by electron-conductive minerals such as pyrite or near-surface interference [17].

Limited by the data frequency band and noise, the inversion stability of the time constant (τ) and frequency exponent (c) is insufficient in this dataset; therefore, only η is used as the first-order screening indicator in this study, and cross-constraints from the resistivity structure are incorporated in the geological interpretation. In addition, clay content and disseminated sulfide minerals (e.g., pyrite) can also contribute to the observed polarizability response; these contributions are distinguished from hydrocarbon-related

anomalies mainly in combination with structural morphology, and the selection of favorable hydrocarbon zones relies on the joint interpretation of polarizability anomalies and the resistivity profile, rather than on polarizability alone. More generally, induced-polarization and complex-resistivity responses are affected by various electrochemical and mineralogical processes, and the "polarizability anomaly + resistivity trap" joint criterion adopted in this paper is intended precisely to reduce this multiplicity.

Therefore, the "polarizability anomaly + resistivity trap" superposition evaluation approach adopted in this paper is crucial. Only targets with both good trap conditions and polarizability anomalies are identified as first-class favorable zones. For example, the perfect superposition of anomaly No. 5 with the anticlinal structure in the Yecheng sag greatly enhances its exploration value (Figure 6). The anomalies Nos. 17, 18, and 20 on the Maigaiti slope are also mostly associated with local structural highs, reducing the multiplicity risk of a single parameter. Nevertheless, the coincidence of polarizability anomalies with structural highs cannot uniquely determine the origin of the anomalies; other causes (pyritization, clay content, and near-surface interference) cannot be completely excluded, and drilling verification is required. Conversely, where structural highs overlap with polarizability anomalies, the credibility of the favorable zones is enhanced relative to single-parameter predictions.

5.3. Method Effectiveness

The successful application of TFEM in this area demonstrates that this method can simultaneously provide resistivity parameters reflecting deep structure and polarizability parameters indicating hydrocarbon potential. Through time–frequency dual-domain joint inversion and well-seismic constraints, the interpretability of deep targets has been improved [15,19,27]. A direct comparison with seismic data supports this conclusion: on the north–south seismic profiles across the SW Tarim Depression, deep reflections from the Precambrian strata are unclear (Figure 8), whereas the TFEM resistivity profile provides a continuous depiction of the deep electrical structure, demonstrating the effectiveness of the resistivity structural profile for deep structural characterization in this area. In areas like the SW Tarim Depression with low exploration maturity and limited seismic data quality, TFEM can therefore serve as an effective complementary means for rapid evaluation of deep to ultra-deep exploration potential.

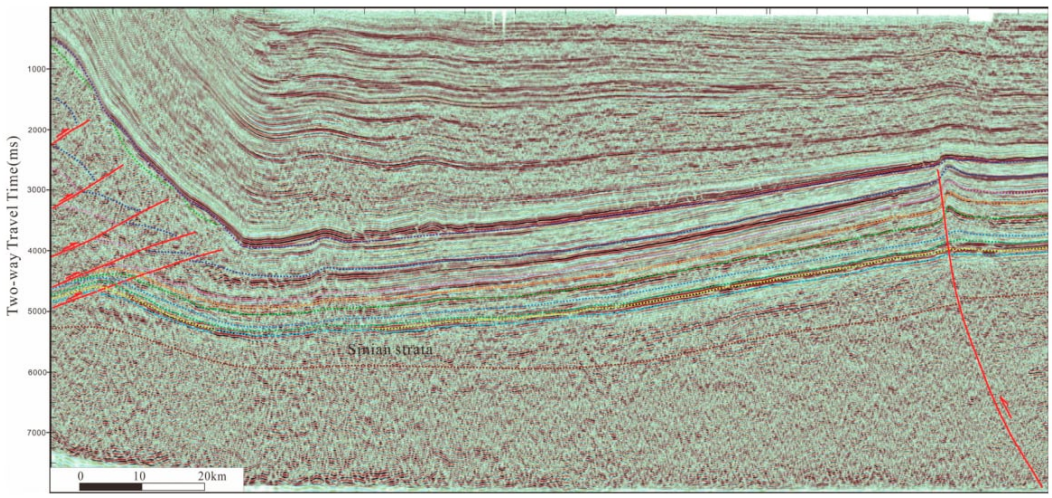

Figure 8. North–south seismic profiles across the SW Tarim Depression show unclear seismic reflections from the deep Precambrian strata [22].

5.4. Implications of Deep Structure for Hydrocarbon Accumulation

The "three-zone" structure revealed in this study clarifies the differences in hydrocarbon accumulation conditions among different structural units. The West Kunlun thrust belt is strongly reworked by faults; although it is near the source, trap preservation conditions are complex, and finding relatively stable fault blocks or anticlines formed in late stages is key. The deep part of the Yecheng sag has potential source rocks (e.g., dark mudstones in the Precambrian aulacogen [27]), and the intra-sag uplift anticline is a long-term migration direction for oil and gas. Moreover, the overlying thick Cenozoic provides good sealing, forming the basis for large oil and gas fields. The Maigaiti slope is a favorable direction for lateral hydrocarbon migration, with faults and unconformities forming an efficient carrier network. Searching for targets related to faulted anticlines or stratigraphic–lithologic traps is significant. In particular, the discovery of Precambrian aulacogens further extends exploration series to deep and ultra-deep layers, and their interior may develop Sinian–Cambrian accumulation assemblages similar to the Anyue gas field in the Sichuan Basin [28], worthy of long-term exploration.

The present structural configuration of the SW Tarim Depression records superimposed deformation of multiple stages: extensional rifting formed the aulacogens during the Nanhua–Sinian period; differential subsidence prevailed during the Paleozoic; uplift of the Bachu Uplift in the northern part of the depression from the Permian to the Triassic caused the strata to thin northward—(the southward-thickening geometry of the Permian in the Yecheng sag therefore mainly reflects this northern uplift rather than purely original depositional thickening); Indosinian–Yanshanian tectonic adjustment followed; and Cenozoic thrusting of the West Kunlun orogenic system, together with flexural subsidence that deposited a 7000–10,000 m molasse succession in the sag since the Neogene, further modified the configuration [5,7,21]. Therefore, the TFEM profile images the present-day electrical structure after this superimposed modification, and reconstruction of the original extensional architecture requires independent methods such as balanced cross-section restoration; the interpretation of a Paleozoic extensional background in this study is accordingly qualified by these later effects.

The deep structural architecture revealed by TFEM exerts a first-order control on the regional petroleum system: the Precambrian rift troughs controlled the distribution of potential source rocks, while structural highs—the intra-sag uplift and the faulted anticlines on the slope—were long-term migration directions for hydrocarbons [13,20].

It should also be noted that faults do not necessarily act exclusively as migration conduits. Depending on their architecture, fault-rock lithology, deformation history, and diagenetic evolution, faults can serve as vertical or lateral fluid migration pathways, hydraulic barriers, compartment boundaries, or temporary conduits during specific tectonic periods. Therefore, not all interpreted faults in this study are considered effective hydrocarbon migration pathways; their effectiveness is evaluated mainly according to the match between fault activity periods and hydrocarbon accumulation periods.

In addition, the analogy with the Anyue gas field in the Sichuan Basin is limited to the type of accumulation assemblage. Major geological differences exist between the two areas: the Sinian–Cambrian petroleum system of the Sichuan Basin developed on a cratonic platform with dolomite reservoirs along paleo-uplift margins, whereas the Tarim aulacogens were filled in a rift setting and have been strongly modified by Cenozoic thrusting; the depositional systems, trap styles, and preservation conditions therefore differ, and the analogy should be treated with caution.

Regarding the preferred exploration intervals, the Carboniferous consists of normal shallow-marine shelf carbonates interbedded with mudstone and fine clastic rocks (~1800 m); the Permian comprises marine dark mudstone and siltstone interbedded with sandstone and

locally basalt, passing upward into continental red beds (500–1200 m); and the Silurian–Devonian consists of littoral–neritic variegated clastic rocks (1000–2000 m) [9–13]. The development of reservoirs in these intervals is controlled by depositional environment, facies distribution, lithological variability, and stratigraphic architecture: the Carboniferous–Permian combines marine carbonate and clastic reservoirs with regionally developed mudstone seals, and the Silurian–Devonian clastics can form favorable reservoir–seal pairs with intraformational mudstones, which together constitute the sedimentological basis for preferring these intervals. Studies of sedimentary facies and depositional architecture, such as the analysis of the Maastrichtian Pab Formation by Mehmood et al. [29], provide a useful methodological framework for understanding how facies and depositional architecture control reservoir distribution; this reference is cited as a conceptual and methodological analogy and does not imply that the same depositional systems are present in the SW Tarim Depression.

Consistent with the accumulation model proposed by Zhao Feng [13] that "the Lower Cambrian Yuertusi Formation and Cambrian–Ordovician dolomite constitute accumulation assemblages, faults connect sources, and reservoirs control enrichment," the intra-sag uplift in the Yecheng sag and the faulted anticlines in the Maigaiti slope selected in this study are both located near the structural hinge zones of paleo-uplift migration. These areas have well-developed faults and unconformities, favorable for hydrocarbon migration, accumulation, and preservation.

5.5. Limitations

Several limitations of the methodology should be acknowledged: (1) electromagnetic inversion is inherently non-unique, and different subsurface distributions of electrical properties can produce similar observed responses; (2) although the regularized OCCAM inversion adopted here is relatively insensitive to the initial model, the inversion results still depend to some extent on the choice of initial model and constraints; (3) noise and data coverage impose limits—the 200 m station spacing constrains the lateral resolution of deep targets, and the legacy data, acquired with older instruments and fewer frequencies, have limited ability to resolve deep structures even after reprocessing, so that some segments of the composite profile cannot meet the needs of fine stratigraphic characterization; (4) there is a trade-off between model smoothness and structural resolution, and smooth inversions may underestimate thin layers and steeply dipping interfaces; (5) the ability to resolve steeply dipping faults is limited; (6) the depth estimation of deep stratigraphic boundaries carries uncertainty; and (7) combining electromagnetic datasets acquired in different vintages and with different systems (TFEM and MT) introduces additional uncertainty. These limitations should be considered when applying the interpretations presented here. In particular, because different lithologies may exhibit similar resistivity and smooth inversion blurs boundary positions, stratigraphic boundaries identified from the resistivity profile in segments without well or seismic control should be regarded as interpretations rather than determinations.

5.6. Synthesis of New Insights

To highlight the take-home message and the new contributions of this study, a synthetic summary figure (Figure 9) is presented. Compared with previous knowledge, the main new insights are as follows: (1) The Lower Paleozoic in the SW Tarim Depression exhibits a clear "three-zone" structural pattern, with the central Yecheng sag being a deeply buried, southward-thickening depression that has not been previously well imaged. (2) The NE-trending Precambrian aulacogens previously inferred from seismic data are further constrained by TFEM, which provides independent electrical evidence for their width, asymmetry, and contact relationships with the overlying strata, thereby extending the ex-

ploration targets to the Nanhua–Sinian. (3) The superposition of polarizability anomalies with structural highs (intra-sag uplift and faulted anticlines) reveals that the most favorable hydrocarbon zones are controlled by both deep structure and fluid distribution. These findings provide a new geological model for hydrocarbon accumulation in the deep part of the SW Tarim Depression and suggest that the intra-sag uplift and the middle Maigaiti slope are the most promising targets for future exploration.

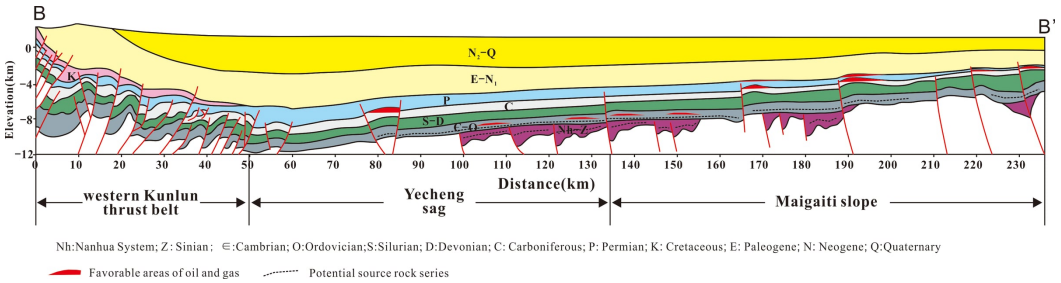

Figure 9. Synthetic summary diagram showing the deep structural framework, Precambrian aulacogen distribution, and favorable hydrocarbon zones in the SW Tarim Depression, highlighting the new understanding gained in this study. The geological model shown integrates the TFEM interpretations of this study with previously established regional geology.

6. Conclusions

(1) Direct geophysical observations: The TFEM resistivity inversion profile reveals the deep electrical structure of the SW Tarim Depression, and the polarizability inversion profile delineates 20 strong polarizability anomalies (Class I and II), which are concentrated in the Yecheng sag and the middle section of the Maigaiti slope and are most developed within the Carboniferous–Permian.

(2) Geological interpretation: Based on these observations and well-log calibration, the Lower Paleozoic is interpreted to comprise three structural zones from south to north—the West Kunlun thrust belt (imbricate thrusts), the Yecheng sag (a deeply buried sag thickening southward), and the Maigaiti slope (a broad gentle slope rising northward). The wedge-shaped low-resistivity bodies in the Precambrian are interpreted as Nanhua–Sinian aulacogen fills controlled by normal faults, although alternative explanations cannot be entirely excluded. Their genetic link to the breakup of the Rodinia supercontinent is a regional inference based on published tectonic models and regional correlations [25], for which this study provides no independent chronological constraints.

(3) Preliminary exploration prediction: Based on the above geophysical observations and geological interpretations (rather than direct evidence), the intra-sag uplift anticline belt in the Yecheng sag and the faulted anticline development belt in the middle section of the Maigaiti slope are predicted as the most favorable exploration zones, with the Carboniferous and Permian as the most favorable layers, the Silurian–Devonian as potential replacement series, and the new series within the Precambrian aulacogens worthy of long-term attention; all predicted targets require verification by future drilling. This study demonstrates the applicability of TFEM to the rapid evaluation of deep to ultra-deep targets in areas with low exploration maturity, and the "structure-fluid" superposition relationship revealed provides a new exploration direction for the SW Tarim Depression.

Author Contributions: Conceptualization, L.W., W.M. and Y.X.; methodology, D.Z. and Y.L.; software, D.Z.; investigation, L.W., Y.L. and Y.Y.; resources, L.W.; writing—original draft preparation, L.W.; writing—review and editing, Y.X.; visualization, W.M. and Y.Y.. All authors have read and agreed to the published version of the manuscript.

Funding: This research was funded by the Geological Survey Project of China Geological Survey, grant numbers DD20240052, DD20242510, DD20230021 and DD20190090.

Data Availability Statement: The publicly available data presented in this study are contained within the article.

Conflicts of Interest: The authors declare no conflicts of interest.

Abbreviations

The following abbreviations are used in this manuscript:

TFEM	Time–Frequency Electromagnetic Method
SW	Southwestern

References

1. Jia, C.Z. *Tectonic Characteristics and Oil & Gas in Tarim Basin, China*; Petroleum Industry Press: Beijing, China, 1997.
2. He, D.F.; Li, D.S.; He, J.Y.; Wu, X.Z. Comparison in petroleum geology between Kuqa depression and southwest depression in Tarim Basin and its exploration significance. *Acta Pet. Sin.* **2013**, *34*, 201–218.
3. Wang, Q.H.; Xu, Z.P.; Zhang, R.H.; Yang, H.J.; Yang, X.Z. New fields, new types of hydrocarbon explorations and their resource potentials in Tarim Basin. *Acta Pet. Sin.* **2024**, *45*, 15–32.
4. Yang, H.J.; Xu, Z.P.; Yang, X.Z.; Tang, Y.G.; Mo, T.; Chen, C.; Xie, Z.; Luo, X.S.; Wang, B. Progress in oil and gas exploration during the 14th Five-Year Plan period and future exploration orientation in Tarim Basin. *China Pet. Explor.* **2026**, *31*, 80–99.
5. Hu, W.S.; Chen, Y.S.; Xiao, A.C.; Liu, X.F.; Liu, S.G. Structural evolution and petroleum systems in the SW Tarim Depression of Tarim Basin. *Pet. Explor. Dev.* **1997**, *1*, 14-17+92. Available online: https://kns.cnki.net/kcms2/article/abstract?v=GJlEMrJefi-C4htbnNrSFyJIDYJyeMU2wRaQdC35G892khSvm4PUj1E0aUhd7nVXqZ36Z49yRJ294079vPOpsn_v8WSB94eI7z72FOYnc5ii8KCUVR0NcB-47k00CTIRzEnHPyBy4hlPet8FLXCdwMT69OqwmQfddGaWB2exqSQMcWoPhsB8MQ== (accessed on 1 November 2026).
6. Cao, Z.C.; Jiang, H.S.; Zhang, J.C.; Geng, F.; Sha, X.G.; Hao, J.L.; Li, T.; Guo, X.W.; Tao, Z. Structure and evolution of Precambrian basement in southwestern Tarim Basin. *Pet. Geol. Exp.* **2023**, *45*, 844–856.
7. Fan, X.G.; Cheng, X.G.; Chen, H.L.; Wang, C.; Wang, C.Y. Basin-range coupling structure and deformation features of the eastern Cenozoic foreland basin in SW Tarim. *Geotecton. Metallog.* **2015**, *39*, 241–249.
8. Tian, L.; Zhang, H.Q.; Liu, J.; Zhang, N.C.; Shi, X.Q. Distribution of Nanhua-Sinian rifts and prototype basin evolution in southwestern Tarim Basin. *Pet. Explor. Dev.* **2020**, *47*, 1122–1133. [CrossRef]
9. Zhang, L.; Zeng, C.M.; Zhu, L.C.; Feng, X.J.; Chen, C. Discussion on accumulation conditions of Miocene condensate gas in Guman structural belt, Yecheng sag. *Xinjiang Pet. Nat. Gas.* **2014**, *10*, 1–5.
10. Meng, M.M.; Kang, Z.H.; Liu, J.J.; Zhou, L.; Liu, Z.; Qiu, H.J. Research on the sedimentary characteristics of Permian in Yecheng-Hetian area of southwest Tarim Basin. *J. Chongqing Univ. Sci. Technol. (Nat. Sci. Ed.)* **2013**, *15*, 39–44.
11. Du, Z.L.; Zeng, C.M.; Qiu, H.J.; Yang, Y.X.; Zhang, L. Key formations of the Permian hydrocarbon source rocks and oil-source correlation of well KD1 in Yecheng depression of southwestern Tarim Basin. *J. Jilin Univ. (Earth Sci. Ed.)* **2016**, *46*, 651–660.
12. Zhu, G.Y.; Chen, F.R.; Chen, Z.Y.; Zhang, Y.; Xing, X.; Tao, X.W.; Ma, D.B. Discovery and basic characteristics of the high-quality source rocks of the Cambrian Yuertusi Formation in Tarim Basin. *Nat. Gas. Geosci.* **2016**, *27*, 8–21.
13. Zhao, F. Formation, evolution and petroleum exploration significance of Lower Paleozoic paleo-uplift in southwest Tarim Depression. Master's thesis, China University of Petroleum, Beijing, China, 2019.
14. He, Z.X.; Chen, Z.C.; Ren, W.J.; Pang, H.C.; Tian, Z.Q.; Shen, Y.B. Time-frequency electromagnetic (TFEM) exploration technology: Data acquisition system. *Oil Geophys. Prospect.* **2020**, *55*, 1131–1138.
15. He, Z.X.; Hu, Z.Z.; Wang, Z.G.; Zhao, Y.S.; Shen, Y.B.; Liu, X.J. Time-frequency electromagnetic (TFEM) technique: Step-by-step constraint inversion based on artificial fish swarm algorithm. *Oil Geophys. Prospect.* **2020**, *55*, 898–905.
16. He, Z.X.; Chen, T.; Chen, B.C.; Shi, Y.L.; Liu, X.J.; Chen, X.F. Time-frequency electromagnetic techniques: Hydrocarbon detection principle and methods. *Oil Geophys. Prospect.* **2025**, *60*, 1032–1045.

17. Li, Z.B.; Liu, S.X.; Wang, Y.J. Application foundation and prospect of induced polarization method in oil and gas exploration. *Geophys. Prospect. Pet.* **2005**, *44*, 409–414.
18. Li, Y.; Chen, C.; Feng, X.J.; Zhang, L.; Zeng, C.M.; Fan, Q.H. New discovery of Nanhuaian rift system in southwestern Tarim Basin and its geological significance. *Acta Petrol. Sin.* **2016**, *32*, 825–832.
19. He, Z.X.; Dong, W.B.; Zhao, G.; Hou, Y.J.; Shen, Y.B.; Liu, X.J. Time-frequency electromagnetic (TFEM) technology: Data processing. *Oil Geophys. Prospect.* **2021**, *56*, 1391–1399.
20. Cui, H.F.; Tian, L.; Zhang, N.C.; Liu, J. Characteristics of Ordovician hydrocarbon accumulation in Maigaiti slope of southwest Tarim Depression. *Nat. Gas. Geosci.* **2016**, *27*, 22–30.
21. Yang, G.; Chen, Z.X. Two-stage evolution model of wedge structure and strike-slip structure superimposition in Qimugen, southwestern Tarim. *Chin. J. Geol.* **2023**, *58*, 347–378.
22. Bai, Z.K.; Wang, M.J.; Gao, Y.J.; Zhang, J.F.; Zhou, X.G.; Han, M.; Yang, Y.X.; Sun, S.Z.; Cheng, M.H.; Geng, F.; et al. *Atlas of Deep Geological Structural Characteristics in the Tarim Basin*; Petroleum Industry Press: Beijing, China, 2023.
23. He, Z.X.; Yang, G.S.; Chen, S.Q.; Zhao, G.; Liu, Z.H.; Guo, R.W. Time-frequency electromagnetic (TFEM) method: Data acquisition design. *Oil Geophys. Prospect.* **2019**, *54*, 908–914.
24. Cole, K.S.; Cole, R.H. Dispersion and absorption in dielectrics I. Alternating current characteristics. *J. Chem. Phys.* **1941**, *9*, 341–351. [CrossRef]
25. He, B.Z.; Jiao, C.L.; Huang, T.Z.; Zhou, X.; Cai, Z.; Cao, Z.; Jiang, Z.; Cui, J.; Yu, Z.; Chen, W.; et al. Structural architecture of Neoproterozoic rifting depression groups in the Tarim Basin and their formation dynamics. *Sci. China Earth Sci.* **2019**, *62*, 529–549. [CrossRef]
26. Wang, Z.G.; He, Z.X.; Qin, J.C.; Wang, Z.H.; Zhang, L.; Zhang, Y.F. Advances of TFEM technique and its application. *Oil Geophys. Prospect.* **2016**, *51*, 144–151.
27. Qu, Y.; Yang, Y.H.; Li, L.; Tang, Q.Q.; Sun, D.; Luo, Q.; Ge, D.Z. Application of continuous electromagnetic profiling method to the exploration of a rift depression in Maigaiti slope, Tarim Basin. *J. Chengdu Univ. Technol. (Sci. Technol. Ed.)* **2024**, *51*, 152–163.
28. Zou, C.N.; Du, J.H.; Xu, C.C.; Wang, Z.C.; Zhang, B.M.; Wei, G.Q.; Wang, T.S.; Yao, G.S.; Deng, S.H.; Liu, J.J.; et al. Formation, distribution, resource potential and discovery of the Sinian-Cambrian giant gas field, Sichuan Basin, SW China. *Pet. Explor. Dev.* **2014**, *41*, 278–293. [CrossRef]
29. Mehmood, M.; Naseem, A.A.; Saleem, M.; Rehman, J.U.; Kontakiotis, G.; Janjuhah, H.T.; Khan, E.U.; Antonarakou, A.; Khan, I.; Rehman, A.U.; et al. Sedimentary Facies, Architectural Elements, and Depositional Environments of the Maastrichtian Pab Formation in the Rakhi Gorge, Eastern Sulaiman Ranges, Pakistan. *J. Mar. Sci. Eng.* **2023**, *11*, 726. [CrossRef]

Disclaimer/Publisher's Note: The statements, opinions and data contained in all publications are solely those of the individual author(s) and contributor(s) and not of MDPI and/or the editor(s). MDPI and/or the editor(s) disclaim responsibility for any injury to people or property resulting from any ideas, methods, instructions or products referred to in the content.